A Comparative Study on the Induced Current Density in Humans Exposed to ELF Electric Fields

Vitantonio Amoruso, Giovanna Calò, Francesco Lattarulo, Dragan Poljak, Andres Peratta, Cristina Gonzalez

Abstract: **A comparison between two theoretical methods, recently adopted for evaluating induced currents in a human body, is here presented. In both cases, a vertical ELF electric field is assumed for the coupling to a standard human subject. Specifically, the diakoptic method (DM), applied to a homogeneous multi-sphere model of man with low partitioning degree, and the Boundary Element Method (BEM), applied to a non-homogeneous model with high partitioning degree, have been selected. The analytical and numerical formulations, respectively distinctive of the above methods, are carefully described and a number of data are reported and commented upon.**

***Index terms*: Boundary Element Method, diakoptic method, ELF human exposure, induced currents**

I. INTRODUCTION

The electromagnetic fields produced at extremely low frequency (ELF) by power installations, at radiofrequency for radio and television broadcasting and at microwaves by GSM mobile phones are of primary interest regarding environmental problems involving human beings.

Assessing the radiation hazard is still an open problem at ELFs since the currently claimed correlation between exposure and serious pathologies, such as neoplastic disease [1]-[4], is still subject to debate. The above harmful correlation essentially derives from some epidemiological studies on involved population groups. On the other hand, a large amount of laboratory research on ELF-field carcinogenesis has so far produced controversial results.

A human body exposed to electric fields,is subject to an induced current. In the high frequency range, specific absorption rate (SAR) and temperature increase in the tissue due to electromagnetic effects are good indicators of exposure intensity. However, in the quasistatic case, the resultant internal electric fields and current densities, mutually correlated by means of the tissue conductivity, are often considered as exposure indicators, this is due to the negligible thermal effects at low frequency and field intensities.

The current distribution on the exposed surface of the human body is essentially non-uniform and strongly dependent on the actual exposure conditions, namely on the field orientation and magnitude and the human body's size, posture, connection to ground and relative position with respect to influencing nearby conductors. In the following, reference will only be made to the canonical case study of a grounded man either isolated from or above a conducting plane (no presence of nearby conductors appart from the plane will be taken into account).

At ELFs, the human body behaves essentiatlly as a perfect conductor from a point of view external to it, and as a pure resistance from an internal point of view. Moreover, provided that inner conductance inhomogeneities can be disregarded (see, later, Sect V), the internal current density only results dependent on the body configuration. This implies that the prerequisite for a good reproduction of a human exposure to a quasistatic electric field reduces to assigning an optimum sophistication degree to a perfectly conducting model of man.

Either analytical [1]-[2], [5-6], or numerical techniques [7-10] have previously been developed for evaluating, with different degree of accuracy, the current density induced by ELF exposures. To this end, oversimplified [6, 10] and, on the other hand, computationally expensive solvers, the latter often based on the Finite Element Method (FEM) [8] and Finite Difference Time Domain (FDTD) method [7], [9], have been adopted.

This paper aims to compare the features of a pair of so far overlooked, even though efficient, methods. One of them applies the Diakoptic method (DM) [10]-[11] to the human dosimetry after having adopted a low partitioning degree to a human model externally behaving as a perfect conductor. The assumed homogeneity of the internal conductivity also contributes to make the computational effort required quite modest. Such a performance especially promotes investigations on the dynamic dosimetry, namely the theoretical monitoring of the induced current distribution when the human posture progressively changes.

The Boundary Element Method (BEM) [14], has also been applied with success to the problem of human exposure to ELF fields [13],[15]. BEM results more involved than a computationally equivalent FDTD but less expensive than FEM at equal sophistication degree assumed for the object representation. Another attractive feature of BEM is that it avoids a volume mesh discretisation. The formulation is based on the quasi-static approximation of the electric field and the related equation of continuity. The general continuity equation is simplified to the Laplace equation form for the

Manuscript received September 16, 2006 and revised November 20, 2006.

V. Amoruso, G. Calò and F. Lattarulo are with Politecnico di Bari, Dipartimento di Elettrotecnica ed Elettronica, Bari, Italy (e-mail: lattarulo@poliba.it).

D. Poljak is with the University of Split, Department of Electronics, Split, Croatia (e-mail: dpoljak@fesb.hr).

A.Peratta and C. Gonzalez are both with the Wessex Institute of Technology, UK (e-mail: aperatta@wessex.ac.uk).

electric scalar potential, which is numerically handled via BEM with the domain decomposition concept [14]. BEM will accommodate inner conducting inhomogeneities, a supplementary general feature which will be discussed with specific application to ELF studies.

II. Analytical and Numerical Models of the Human Body

A. Diakoptic Theory

The DM applied to the analysis of composite electrode structures offers an efficient and effective solution to electrostatic or quasi-static problems, regardless of the complexity of the system under examination and the low degree of partialisation a priori adopted. According to the original Greek word διαχὸπτω (to cut), the diakoptic method is based on initially tearing a connected structure into large dimensioned elemental blocks. In other words, the exposed human body is assimilated to a multi-element receiving antenna whose elemental blocks are electrically small although comparable with the main anatomic parts. The current contribution of each single element, represented by an equivalent capacitance, takes into account the influence of the remaining elements which compose the overall structure. In fact, the analogical network representation is simply given by the parallel of a set of equivalent capacitances to ground C_{eqi}, therefore, each fed by a driving voltage taking into account the electrostatic height of the overall system.

The human body has been modelled by considering eleven perfectly conducting spheres arranged, as depicted in Fig.1 (a), to simulate any articulate human attitude.

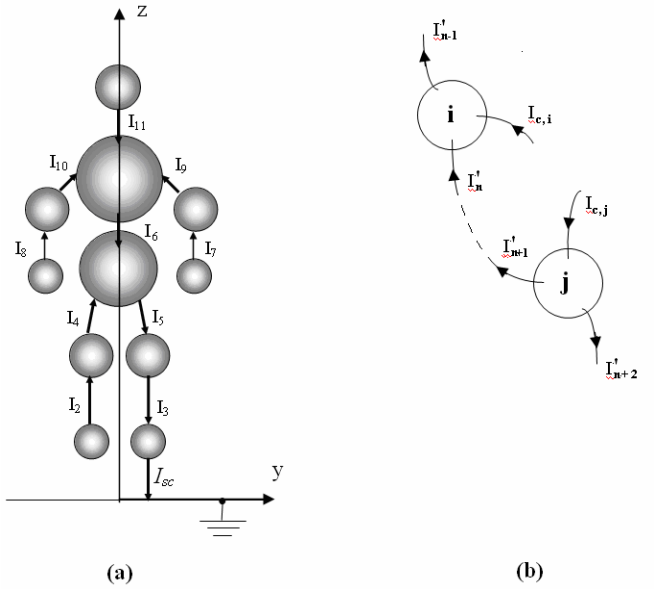

Fig. 1. Diakoptic model of the human body: a) multi-sphere assembled structure, b) i-th and j-th spherical element after diakopting the wiring terminal.

The model requires to be imaged owing to the presence of the conducting plane. Each sphere is dimensioned according to anthropometric criteria applied to a 1.75-m tall subject. The connection between nearby spheres are ensured by unperturbing wires, see Fig. 1 a).

By virtue of the diakoptic theory, the originally assembled structure, represented by eleven spheres, is subdivided into as many elements by cutting the wiring terminals.

More precisely, Fig. 1 (b) shows two generic spherical elements, numbered with i and j (i, j=1..11), obtained by diakopting, i.e. cutting, the connecting wire (dashed line). Therefore, each current-carrying junction is replaced by two terminals, to which a pair of unphysical currents, $I_n^{'}$ and $I_{n+1}^{'}$, feeding the i-th and the j-th spherical elements, respectively, are impressed. According to the adopted numbering, the currents $I_n^{'}$ impressed at the diakopted connecting wires are specified by n= 1…N_t, with $N_t \geq N$. A further feeding terminal attached to the i-th spherical element, see Fig. 1 (b), is accounted for by the partial current $I_{c,i}$ capacitively collected by each i-th portion composing the body exposed to an ELF field. Of course, owing to the electric image of the multi-sphere model, the overall number of impressed currents becomes $2N_t$.

The performances of the diakopted structure are restored by imposing equality of the scalar potentials at the interconnected terminals and current continuity at each junction. An interconnection matrix [*M*] enforces the relation

$$\left[I^{'}\right]=\left[M\right]\ \ \left[I\right] \qquad (1)$$

between the sets of currents $I_n^{'}$ impressed at the diakopted terminals and that of unknown junction currents I_n.

The generic element of [*M*] is 1 (or -1) if the current enters (or leaves) the terminal, otherwise it is zeroed.

Similarly,

$$\left[V\right]=\left[M\right]^T\ \ \left[V^{'}\right], \qquad (2)$$

where the transposed matrix $[M]^T$ allows the equality between the scalar potentials [*V*] and [V'], at the interconnected and diakopted terminals, respectively, to hold.

Furthermore,

$$\left[\mathrm{V}^{'}\right]=\left[Z^{*}\right]\ \ \left[\mathrm{I}^{'}\right] \qquad (3)$$

relates the impressed current and corresponding scalar potential vectors $\left[\mathrm{I}^{'}\right]$ and $\left[\mathrm{V}^{'}\right]$, respectively, by the impedance matrix $[Z^*]$.

After denoting with *m* and *n* two generic terminals of the diakopted structure,

$$Z_{mn}^{*}=\frac{1}{j\omega C_{mn}} \qquad (4)$$

can be written to represent the relevant element of the matrix $[Z^*]$. Here,

- C_{mn} is roughly set equal to the self capacitance $C_i = 4\pi\varepsilon_o r_i$ if the *m*-th and *n*-th terminals lie on the same *i*-th sphere (r_i is the radius of the i-th sphere);
- C_{mn} is roughly calculated as $C_{ij} = 4\pi\varepsilon_o d_{ij}$ if the *m*-th and *n*-th terminals lie on *i*-th and *j*-th spheres, respectively (d_{ij} is the inter-centre distance between the i-th and the j-th elements).

Rearranging eqs. (1) - (4), gives

$$[V] = [M]^T \quad [Z^*] \quad [M] \, [I] \, = [Z] \quad [I] \qquad (5)$$

which represents the governing matrix relation for the assembled multi-element body.

Therefore,

$$[I] = [Z]^{-1} \, [V] = [Y] \, [V] \qquad (6)$$

is the relation giving the vector of junction currents.

Assessment of the current induced in the human body by ELF exposure requires evaluation of the partial currents $I_{c,i}$ capacitively collected by each i-th portion composing the body. Therefore, a set of equivalent capacitances to ground C_{eqi}, each corresponding to a diakopted element, can be calculated to ultimately give the set of collected partial displacement currents.

Imposing Kirchhoff's current law to the terminals feeding the i-th sphere gives

$$C_{eqi} = 2\frac{I_{c,i}}{\omega V_o} = 2\frac{I_{n+1} - I_n}{\omega V_o}$$

Here, C_{eqi} denotes the imaged equivalent capacitances in function of the previously calculated junction currents. Note that such currents are related, by eq. (6), to the self and mutual capacitances of the eleven spheres.

Since the multi-sphere system, equivalent to a person grounded through an impedance Z_g, is exposed to an undisturbed uniform vertical electric field of magnitude E_0, the antenna reciprocity theorem can be evoked under quasi-static conditions for removing the above incident field and impressing a feeding total current I_{sc} equal to that capacitively drained by the system. The current I_{sc} could also be given by applying to the assembled structure a suitable floating voltage V_0. Accordingly,

$$V_0 = h_0 E_0 \qquad (7)$$

where

$$h_o = \frac{\sum_i h_i C_{eq_i}}{C_o} \qquad (8)$$

denotes the electrostatic (or effective) height of the structure. Here,

$$C_o = \sum_i C_{eq_i} \qquad (9)$$

is the total capacitance to ground of the structure and h_i is the electrostatic height of the i-th element. If the structure element issubstantially elevated above the grounded plane, then h_i reduces to the elevation of the geometrical centre. Otherwise, the electrostatic height decreases owing to the proximity to the plane. Using spherical blocks makes such an evaluation quite a canonical exercise.

Accordingly,

$$I_{sc} = \frac{h_0 E_o}{\dot{Z}_o + \dot{Z}_g} \qquad (10)$$

represents the total current, where h_0 and $Z_0 = 1/j\omega C_0$ are derived from Eqs. (8) and (9).

After some manipulations, here omitted for the sake of brevity (see [5-6] and [10] for details),

$$\frac{I_{c,i}}{I_{sc}} = \frac{\omega C_{eq_i} V_0}{\omega V_0 \sum_i C_{eq_i}} = \frac{C_{eq_i}}{C_0} \qquad (11)$$

is the displacement current distribution normalised to the total current.

It is worth conclusively considering how

- the overall calculation (which include partial equivalent capacitances to ground representative of each element of the assembled structure, the total capacitance to ground, the voltage acquired by the assembled structure disconnected from ground and exposed to a uniform electric field, the collected total current and the distribution of junction currents) results developed by an analytically-based, thus inherently self-consistent, method;
- in spite of a preliminary calculation of capacitances C_{mn} affected by first-order error, the method gives a final set of capacitances C_{eqi}, representative of each anatomical block, affected by second-order error (see [10] for more detailed considerations);
- the method inherently neglects internal non-homogeneities, which implies that the final evaluation of the internal current density is only related to cross-sectional data distinctive of a realistic human body.

B. Boundary Element Method for ELF human body exposure

The continuity equation is usually written as follows:

$$\nabla \cdot \vec{J} + \frac{\partial \rho}{\partial t} = 0 \qquad (12)$$

where $\vec{J}$ and ρ represent the current density and the volume charge density, respectively. If the latter is expressed in terms of the scalar potential,

$$\vec{J} = -\sigma \nabla \varphi \qquad (13)$$

in accordance to the differential form of Ohm's Law, in which case σ denotes the conductivity of the medium.

The volume charge density ρ and scalar potential φ are related through the Poisson equation

$$\nabla \cdot (\varepsilon \nabla \varphi) = -\rho \qquad (14)$$

where ε is the permitivity of the medium.

Rearranging eqs. (12)-(14) yields:

$$\nabla \cdot [(\sigma + j\omega\varepsilon)\nabla \varphi] = 0\,, \qquad (15)$$

where time-harmonic ELF exposures with angular frequency $\omega=2\pi f$ has been considered.

In the above frequency range, all organs behave as good conductors, while the surrounding air is a lossless dielectric medium. Solving the Laplace equation (15) in the body region, the induced current density can be obtained from Ohm's Law (13).

The condition for the tangential component of the electric field at the interface between the two media is given by

$$\vec{n} \times (\vec{E}_b - \vec{E}_a) = 0 \qquad (16)$$

where $\vec{n}$ denotes the unit normal to the interface, while the quantities $\vec{E}_a$ and $\vec{E}_b$ represent the fields just outside and inside the human body, respectively.

Expressing the electric field in terms of scalar potential gives

$$\vec{n} \times (\nabla \varphi_b - \nabla \varphi_a) = 0 \qquad (17)$$

If ρ_s is the surface charge density, then the equality

$$\vec{n} \cdot \vec{J} = -j\omega\rho_s \qquad (18)$$

holds as an interface condition for the normal component of the induced current density at the body-air interface.

Substituting eq. (13) into (14) yields

$$\sigma_b \vec{n} \nabla \varphi_b = -j\omega\rho_s \qquad (19)$$

where σ_b is the corresponding tissue conductivity, and φ_b is the scalar potential at the body surface.

The interface condition for the normal component of the electric flux density at the body surface is

$$\vec{n} \cdot \vec{D} = \rho_s \qquad (20)$$

Representing the electric flux density in terms of scalar potential yields

$$\varepsilon_0 \vec{n} \nabla \varphi_a = \rho_s \qquad (21)$$

where φ_a denotes the outer potential in close proximity of the body.

At extremely low frequencies, the dielectric properties can be neglected, i.e. σ>>ωε (all organs behave as good conductors; see Table I where the electrical conductivities for various tissues are summarised) and, accordingly, the Laplace equation in the body reduces to

$$\nabla \cdot (\sigma \nabla \varphi) = 0 \qquad (22)$$

The body is conceived being located between a pair of parallel conducting plates, in the middle of the earthed lower one (upper electrode connected to a high voltage power line). A calculation domain with the related boundary conditions is shown in Fig. 2.

TABLE I
TISSUE CONDUCTIVITIES

Tissue	σ [S/m]
Brain	0.12
Eye	0.11
Heart	0.11
Liver	0.13
Kidney	0.16
Intestine	0.16
Muscle	0.5

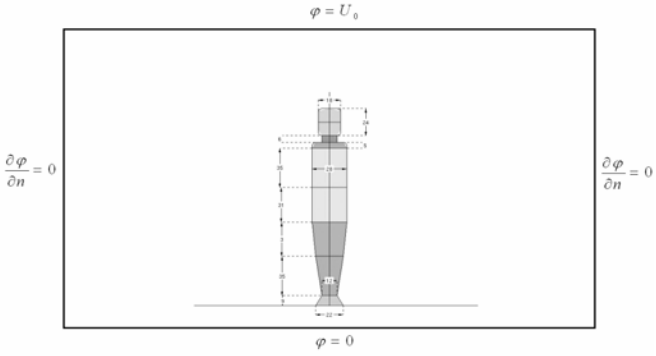

Fig. 2. Calculation domain with the specified boundary conditions.

The different representations of the human body considered are shown in Fig. 3 which shows the main features and dimensions of each model.

Both armless and arms-up models shown in Figs. 3 b)-c) (see [16]) are here taken into account. The prescribed boundary conditions are identical to those used in the case of human being's axialsymmetric multidomain representation.

The Laplace equation, solved by BEM with multi-domain decomposition [13-14], is considered in this section (see [15], [16] for details). The numerical implementation of the BEM requires the discretisation of the domain boundary into elements, and employs the fundamental solution of the leading differential operator. This are the two most powerful advantages of the method, since volumetric discretisations are avoided, and existing knowledge on the equation is incorporated.

By using Green's theorem for scalar functions, the integral representation of eq. (22) applied to a single domain becomes:

$$c(\xi)\varphi(\xi)+\int_{\Gamma_k}\varphi\frac{\partial\varphi^*}{\partial n}d\Gamma=\int_{\Gamma_k}\frac{\partial\varphi}{\partial n}\varphi^* d\Gamma \tag{23}$$

Here φ^* is the three dimensional fundamental solution of Laplace equation, $\partial(\cdot)/\partial n$ is the derivative of $(\cdot)$ in n direction, where n is the outwards normal to the boundary (Γ) of the integration domain (Ω), and c(ξ) is the geometry-dependent term by which the Cauchy type singularity is taken into account.

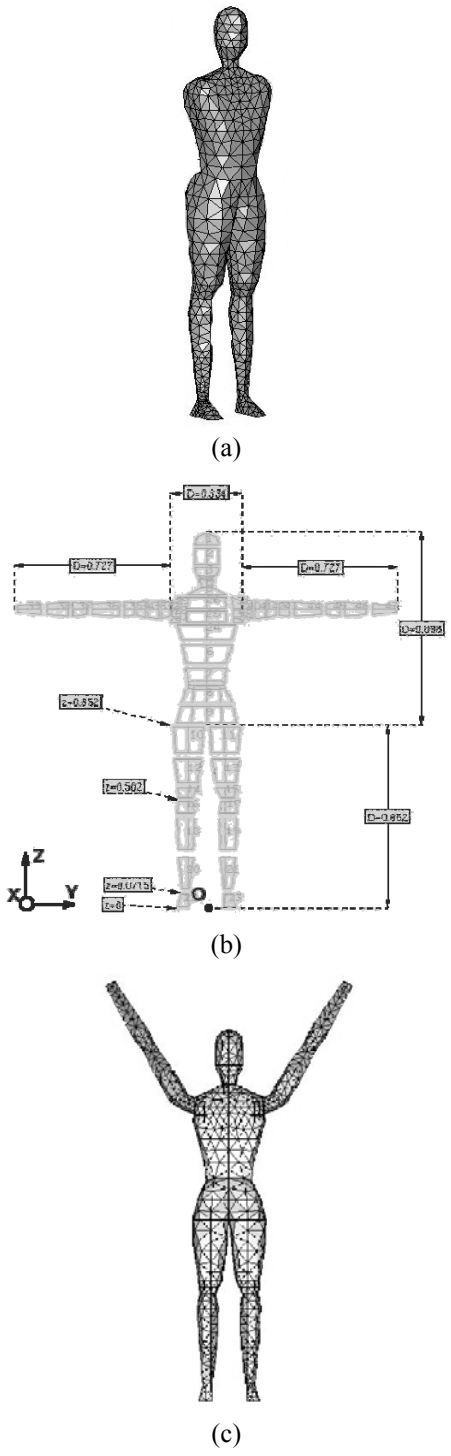

(a)

(b)

(c)

Fig. 3: Meshes and dimensions for the realistic human body models.

The boundary discretisation of eq. (23) into N_k boundary elements yields:

$$c_i\varphi_i+\sum_{j=1}^{N_k}\int_{\Gamma_{k,j}}\varphi\frac{\partial\varphi^*}{\partial n}d\Gamma=\sum_{j=1}^{N_k}\int_{\Gamma_{k,j}}\frac{\partial\varphi}{\partial n}\varphi^* d\Gamma \tag{24}$$

where i and $\Gamma_{k,j}$ stand for source point and j-th boundary element of Ω_k, respectively.

The present implementation of BEM is based on the isoparametric approach with quadratic interpolation functions defined for triangular elements.

The potential, or its normal derivative, at any point of the j-th boundary element, can be written as a linear combination of their corresponding values at the collocation nodes n and the interpolation functions f_n:

$$\varphi(\xi)=\sum_{a=1}^{6}f_n(\xi)\phi_n \quad \text{and} \quad \frac{\partial\varphi(\xi)}{\partial n}=\sum_{a=1}^{6}f_n(\xi)\phi_n \tag{25}$$

The dimensionless coordinate ξ spans from the computational square domain to the triangular element.

Rearranging eqs. (24) and (25) gives the system of equations

$$[\mathrm{H}][\varphi]-[\mathrm{G}]\frac{\partial[\varphi]}{\partial[\mathrm{n}]}=0 \tag{26}$$

for each subdomain; [H] and [G] are matrices defined as follows

$$H_{ij}^n=\int_{\Gamma_{k,j}}f_n\left(\frac{\partial\varphi^*}{\partial n}\right)_j d\Gamma \tag{27}$$

$$G_{ij}^n=\int_{\Gamma_{k,j}}f_n\ \varphi^* d\Gamma \tag{28}$$

if n stands for the collocation nodes inside the j-th observation element. Then, the system of equations arising from each subdomain are assembled in order to build up a closed linear system of equations.

III. Results

On the basis of the above analytical and numerical approaches, different approximation models of the human body, have been considered. The proposed examples are referred to a 1.75-m tall person exposed to a vertically impinging uniform electric field of magnitude E_0=10 kV/m at frequency f=60 Hz. Such a situation typically resembles exposure to overhead power lines.

At first, a simplified geometrical equivalent of the human-body has been considered by roughly approximating the exposed person by a cylinder of height L and radius a=0.14 m, as shown in Fig. 4.

The enhanced sophistication degree distinctive of the model shown in Fig. 2 consists in the fact that a body of revolution with nine blocks, whose overall geometry reproduces a standing person, has been adopted. With respect

to the former oversimplified model, more accurate result derive owing to the anthropomorphic proportions adopted for the different blocks. Therefore, head, neck, torso, legs, ankles, and feet are easily identified whereas the arms are tacitly embodied in the block representative of the torso.

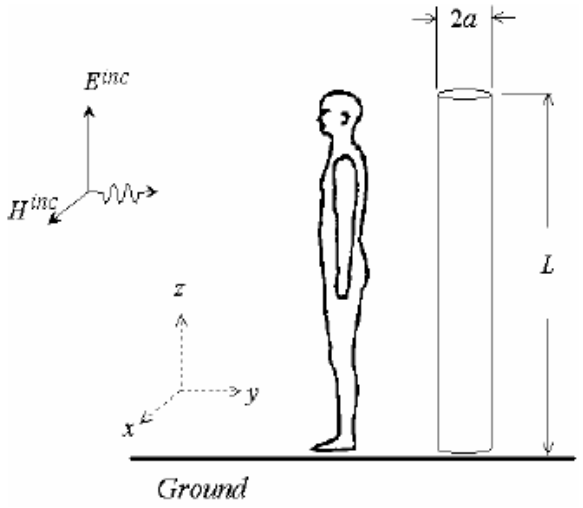

Fig. 4: Cylindrical model of the human body.

Furthermore, two realistic models of human body, without and with arms, are considered in Fig. 3. The accuracy of the model depends on the fact that the system can assume all the possible postures, for example those including side rotation of the arms.

It is worth noticing that dividing the DM-calculated current of each block by its anatomical cross-sectional surface gives the current density averaged in the block volume.

Instead, application of BEM to realistic, anatomically based body models gives the opportunity to capture the position of peaks in the current distribution curve.

A. DM-based results

Fig. 5 shows the calculated current distribution I (circles) and the interpolating curve (solid line), induced in the exposure case of a perfectly grounded person standing with the arms down (α=0) on an earth plane.

In order to compare the results obtained by applying DM and BEM, the current density J has been calculated from the induced current I for the four proposed human models, provided the cross sections are appropriately established on the basis of anatomical data.

Fig. 6 shows the current density J as a function of height h from ground for three human models as specified

1) cylindrical model (dotted curve);
2) revolution-solid model (solid curve),
3) realistic model with arms down: DM-calculated values (asterisks) and corresponding interpolation (dashed curve).

The comparison between the curves in Fig. 6 clearly shows that the cylindrical model of the human body (dotted curve) neglects, as expected owing to its constant cross-section, the high current-density peaks corresponding to the narrow parts, namely neck and ankles. Conversely, both cylindrical (solid curve) and realistic (asterisks and dashed curve) models of the human body manifest an increased current density due to the narrowing sections. On the other hand, the current density increases in the leg region, from h = 0 to 0.8 m, when reference is made to the realistic human body.

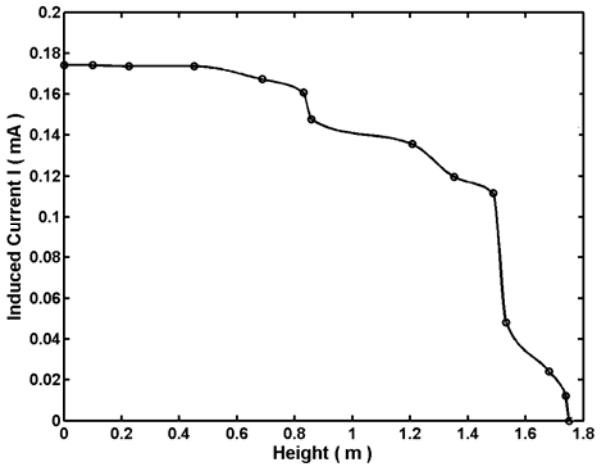

Fig. 5: Induced current I as a function of height from ground, calculated by diakoptic theory (dots) and interpolating curve (solid curve).

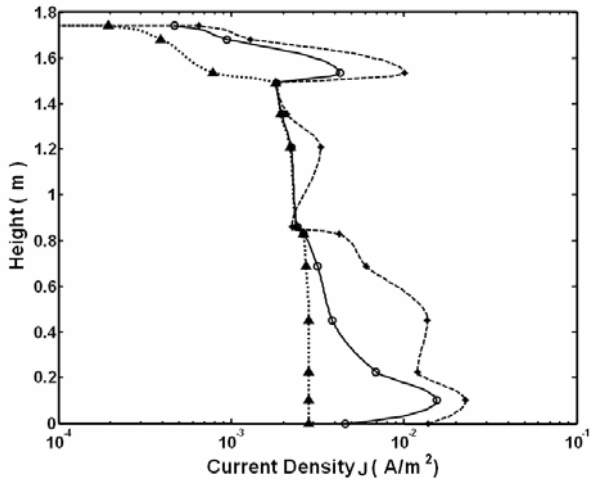

Fig.6: Current density J versus height from ground: calculated values for the cylindrical model (dotted curve), for the revolution-solid model (solid curve), for the realistic model with arms down (asterisks) and corresponding interpolation (dashed curve).

By assuming different postures of the arms, namely a side rotation of angle α, a variation in the induced current density is promoted. Accordingly, Fig. 7 shows the induced current density J, in the region corresponding to head and torso, from h=0.8 to 1.75 m, for two different positions of the arms: arms

down with α=0° (triangles and interpolating dashed curve), arms up with α=120° (circles and interpolating solid curve). It is clear that the side rotation of the arms causes a reduction of the current-density peak in correspondence of the neck, whereas the current density increases in the torso. As a result, the arms can be regarded as causing a screening effect on the head.

Accordingly, it is of remarkable interest to consider the electric field coupling pertaining to animated bodies exposed to ELF. Fig. 8 shows the polar diagrams of the induced current density J in the neck (solid curve), ankle (dashed curve), and elbow (dash-dotted curve) of a standing person whose arms are rotated progressively from α=0° to α=180°.

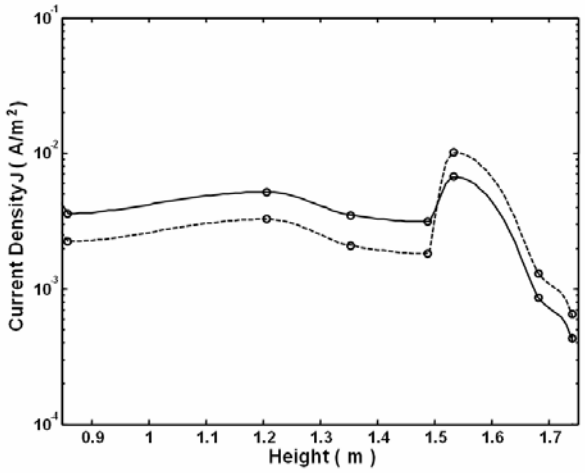

Fig. 7: Induced current density J, in the region corresponding to head and torso, from h=0.8 m to h=1.75 m, for two different positions of the arms: arms down with α=0° (triangles and interpolating dashed curve), arms up with α=120° (circles and interpolating solid curve).

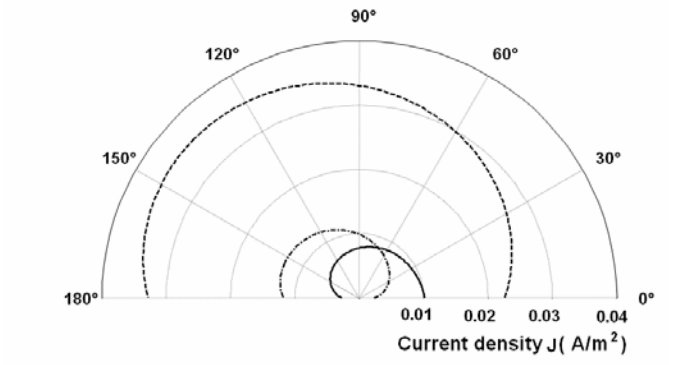

Fig.8: Polar diagrams of the induced current density in the neck (solid curve), ankle (dashed curve), and elbow (dash-dotted curve) of a standing person whose arms are rotated from α=0° to α=180°.

Assuming side rotation of the arms, gives a current density induced in the ankle (dashed curve), which is however a dominant one, subject to a maximum variation of about 36 %. The latter parameter increases with reference to the neck (73 %, dashed curve) and elbow (82 %, dash-dotted curve) sections. Additionally, notes how the curves corresponding to the ankle and elbow assume a complementary behaviour due to the screening effect of the upwardly extending arms.

B. BEM Simulation Results

The corresponding current density distribution for an armless, even though realistic, human body model is shown in Fig. 9. Resurgences of current density peaks, likewise the body of revolution model, is invariably restricted to the ankle and the neck.

A comparison of the current density values obtained via different body models is shown in Fig 10. Analysing the numerical results allows the following conclusions to be drawn:

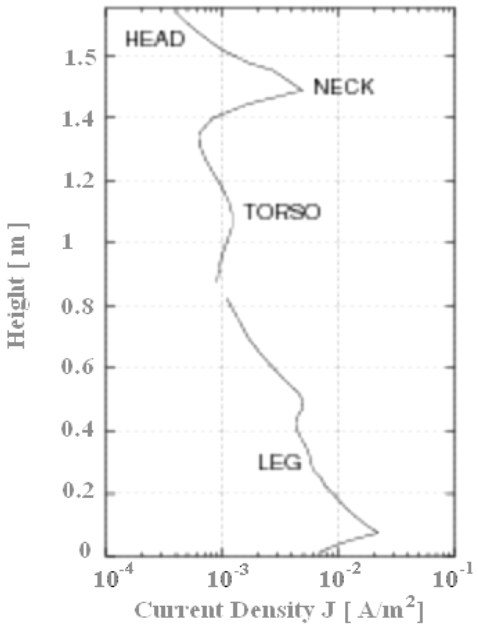

Fig. 9: Distribution of the internal current density.

- in correspondence to restricted cross sections of the human body, a significant increase of the current density occurs, as expected; this is the case for. the discussed peaks in the neck and pelvis;
- extending the arms upwards results in a field shielding at the top, thus causing reduction of current density peak in the neck.
- oversimplified cylindrical representation of the human body suffers from inability to account for the significant increase of the described current density where the cross section gets narrower.

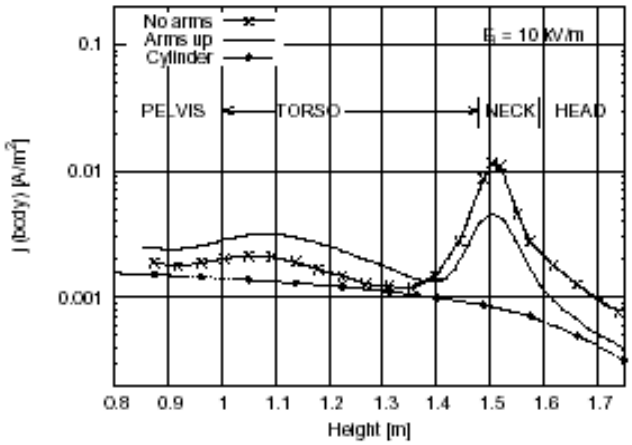

Fig. 10: Induced current density distribution for the various body models.

V. Concluding Remarks

The current densities induced in the human body by a 10-kV/m incident electric field at 60 Hz have been calculated by BEM and DM. Although based on completely different approaches, which are respectively numerical and analytical in nature, both methods proved to be effective in assessing the ELF-exposure effects.

Specifically, the DM allows the induced currents to be evaluated by modelling the human body exposed to ELF field with eleven perfectly conducting spherical elements corresponding to the articulated basic parts of a human body. Anthropometric data are somehow taken into account by adopting surface-equivalent spheres as substitutes of anatomical blocks.

Owing to the low discretization adopted, a feature distinctive of DM, no significant computational effort is required to simulate any articulate attitude. Such a performance is especially suitable for a dynamic dosimetry, as the example recently treated in [16] shows.

Conversely, by applying BEM, the exposed human body has been discretized, as usually is the case when such a method is adopted, by thousands of calculation elements (about 20000), thus giving an extremely detailed description of the induced-current distribution. Additionally, BEM takes into account the electrical conductivities of the various tissues forming a human body.

Tab. II highlights a substantial agreement between the current densities, induced in different anatomical parts, calculated by BEM and DM. Such models effectively reproduce the current density peaks in the narrowing sections, a crucial feature disregarded by oversimplified models. The good reproduction of the results relevant to the neck and pelvis especially proves the slight effect of inner inhomogeneities at low frequency, a performance which has by hindsight taken into account by the described DM. Rather, the result comparison exhibits a moderate departure at the knee and ankle level, namely where larger amounts of capacitively collected upper currents convoy. Such a result tacitly accounts, irrespective of the method and degree of sophistication adopted for the body, for a significant computational sensitivity to the assumed geometry. In fact, adjusting by trial and error the dimensions originally assigned to the single blocks, especially those of larger exposure surfaces, easily gives rise to more impressive data agreements. Such manipulations have deliberately been omitted here owing to the final intent of better appreciating the model features of the methods under examination.

TABLE II
Comparison Between BEM and DM.

	Induced current densities [A/m^2]	
	DM	BEM
neck	0.010	0.011
pelvis	0.002	0.002
knee	0.014	0.010
ankle	0.022	0.030

References

[1] R.W.P King, S.S. Sandler: *Electric Fields and Currents Induced in Organs of the Human body When Exposed to ELF and VLF Electromagnetic Fields*, Radio Sci., Vol. 31, pp. 1153-1167, Sept.-Oct. 1996.

[2] R.W.P. King: *Fields and Currents in the Organs of the Human Body When Exposed to Power Lines and VLF Transmitters*, IEEE Trans. Biomedical Eng., Vol. 45, No 4, pp. 520-530, April 1998.

[3] D.Poljak: "Human Exposure to Electromagnetic Fieds", WIT Press, Southampton-Boston, 2003.

[4] ICNIRP Guidelines for Limiting Exposure to Time-Varying, Electric, Magnetic and Electromagnetic Fields (up to 300GHz), Health Phys., Vol. 74, 4 (1998), 494-522.

[5] V. Amoruso, M. Helali, F. Lattarulo, *An improved model of man for ESD applications*, Journal of Electrostatics, Vol. 49, pp. 225-244, 2000.

[6] V. Amoruso, F. Lattarulo, *ELF electric-field induced currents in the human body*, Alta Freq. Vol. 58, n. 4, pp. 385-390, 1989.

[7] T.W. Dawson, K. Caputa, M.A. Stuchly, *High-Resolution Organ Dosimetry for Human Exposure to Low Frequency Electric Fields*, IEEE Trans. Power Delivery, Vol. 13, No 2, pp. 366-373, April 1998.

[8] A. Chiba, K. Isaka, Y. Yokoi, M. Nagata, M. Kitagav, T. Matsuo, *Application of Finite Element Method to Analysis of Induced Current Densities Inside Human Model Exposed to 60Hz Electric Field*, IEEE Trans. Power Apparatus and Systems, Vol. PAS-103, No. 7, pp 1895-1901, July 1984.

[9] O.P. Gandhi, J.Y. Chen, *Numerical Dosimetry at Power Line Frequencies Using Anatomically Based Models*, Bioelectromagnetics Suppl., Vol. 1, pp. 43-60, 1992.

[10] V. Amoruso, F. Lattarulo, *Diakoptics for electrostatics*, IEE Proc.-Sci. Meas. Technol., Vol. 141, n.5, pp. 317-323, Sept. 1994.

[11] G. Gobau, N.N. Puri, F.K. Schwering, *Diakoptic theory of antennas*, IEEE Trans. Antennas Propag., AP-30, pp.15-26, 1986.
[12] D. Poljak, Y. Rashed, *The Boundary Element Modelling of the Human Body exposed to the ELF Electromagnetic Fields*, Engineering Analysis with Boundary Elements, 26, pp 871-875, 2002.
[13] M.C. Gonzalez, A. Peratta, D. Poljak. *Boundary Element Modelling of the Realistic Human Body Exposed to Extremely Low Frequency (ELF) Electric Fields: Computational and Geometrical Aspects. IEEE Transactions on Electromagnetic Compatibility, 49,(1), 2007*
[14] C.A. Brebbia, J.C.F. Telles, L.C. Wrobel: "Boundary Elements Techniques, Theory and Applications in Engineering", Springer-Verlag, Berlin, Heidelberg, New York, and Tokyo, 1984.
[15] D.Poljak, C.A. Brebbia: Boundary Elements for Electrical Engineers, WIT Pres, Southampton-Boston, 2005.
[16] V. Amoruso, F. Lattarulo: Diakoptic Approach to EMC problems Involving the Human Body, in Electromagnetic Compatibility in Power Systems, F. Lattarulo Ed., Ch 6, Elsevier, Oxford, 2007.

Vitantonio Amoruso 1955, received the degree from the University of Bari in 1980 in Electrical Engineering. He has been a Consultant Engineer and Professor on contract of electrical systems with Department of Electrical Engineering (DEE) of University of Bari. From 1990 to 1999 he has been engineer in charge for the DEE high-voltage laboratory of the Politecnico di Bari. Since 1999 he has been Researcher in Electrical Engineerin and currently he is Associate Professor in Basic Electrical Engineering and Electromagnetic Compatibility. His scientific interest covers some topics of electromagnetic compatibility (lightning and interaction with systems, ESD, bio-hazards) and HVDC corona.

Giovanna Calò was born in Bari, Italy in 1976. She received the Laurea degree in Electronic Engineering and the Ph.D. degree in Electromagnetisms from the Politecnico of Bari, Italy, in 2002 and in 2006, respectively.
In 2002, she joined the Dipartimento di Elettrotecnica ed Elettronica, Politecnico of Bari, where she is currently working on scientific research projects. Her research interests concern biological effects of electromagnetic field, dosimetry, design and characterization of GTEM cells, waveguiding devices, reverberation chambers.

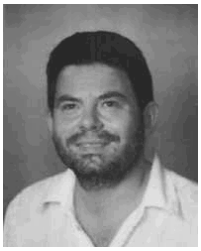

Francesco Lattarulo, 1951, was researcher in High-Voltage Engineering from 1977 to 1985; from 1985 to 1999 he was Associate Professor in Electrotechnology and since 1999 he has been full professor in Fundamentals of Electrical Engineering and Electromagnetic Compatibility. His primary interest is in some topics of applied electrostatics which include EMC and d.c. corona. Dr. Lattarulo has been appointed as a member of the AEI Special Group on EMC and a member of the CEI Technical Committee of EMC.

Dragan Poljak... received his BSc in 1990, his MSc in 1994 and PhD in 1996 from the University of Split, Croatia. He is the Full Professor at the Department of Electronics at the University of Split, and he is also Adjunct Professor at Wessex Institute of Technology, UK. His research interests include frequency and time domain computational methods in electromagnetics, particularly in the numerical modeling of wire antenna structures, and recently numerical modeling applied to environmental aspects of electromagnetic fields. To date Professor Poljak has published more than 180 journal and conference papers in the area of computational electromagnetics, four authored books and one edited book, by WIT Press, Southampton-Boston. Professor Poljak is a member of IEEE, a member of the Editorial Board of the journal Engineering Analysis with Boundary Elements, and co-chairman of the WIT International Conference on Computational Methods in Electrical Engineering and Electromagnetics, and International Conference on Environmental Electromagnetics. He is also editor of the WIT Press Series Advances in Electrical Engineering and Electromagnetics. Recently, professor Poljak was awarded by the National Prize for Science.

Andres Peratta .received his MSc in Physics in 2001 from University of Buenos Aires, Argentina, and his PhD in 2004 from University of Wales, UK. During 2005 he has been a Postdoctoral Fellow and Assistant Professor at the Wessex Institute of Technology (WIT), Southampton UK and became member of the Editorial Board of Journal of Communications, Software and Systems (JCOMSS) sponsored by IEEE and SoftCom Society. In 2006 he became Head of the ICE Division at WIT and ISAC member of the WIT International Conferences on Environmental Electromagnetic Compatibility, Simulation of Electrochemical Processes, and Computational Ballistics. His research interests are Num. Modelling, Boundary and Finite Elements, Electromagnetism and CFD.

Cristina Gonzalez, received her MSc in Physics in 1996 from University of Buenos Aires (Faculty of Exact and Natural Sciences), Argentina.Her background is in Numerical Modelling applied to Electromagnetic problems. She developed her graduate thesis at the Plasma Physics Institute, (INFIP), University of Buenos Aires-CONICET, Argentina, in numerical modelling applied to Nuclear Fusion in Z-pinch experiments. She is currently a Ph.D researcher at the Wessex Institute of Technology. Her thesis is oriented to numerical modelling applied to human exposure to electromagnetic fields.